Analysis of Amplitude Information from 2006 BCAL Cosmics Runs

Andrei Semenov, Zisis Papandreou, and Irina Semenova
University of Regina

1 Data Set

This note describes an analysis of amplitude information in four BCal cosmics run that were taken at Jefferson Lab in 2006: run 2458 (the trigger/paddle was positioned in +100 cm from the center of the calorimeter), run 2459 (+150 cm), run 2475 (-50 cm), and run 2476 (-150 cm). The correspondent *bcal_dst024##.root* files were taken from */work/halld/bcal06* directory. The time information in the *bcal_dst024##.root* files was not used.

2 Pedestals Check

The calorimeter consists of 18 segments; the segments were arranged in vertical 6 columns (of 3 segments each). To select the pedestals in the certain segment in some of the columns, we require the low amplitudes (viz., $adc < 10$) in the 2 remaining segments of the column of interest as well as in all segments of the left neighbour and the right neighbour columns (see Fig.1). The pedestals observed from the most of the segments form compact peaks though the abnormal-shaped pedestals were observed in some segments (see Fig.2).

Fig.3 shows the mean pedestal values extracted from all 18 segments in 4 runs for North-side PMTs (top panel) and South-side PMTs (bottom panel). Run-by-run shifts of pedestals were clearly observed, and all amplitudes in the following analysis were pedestal-corrected on run-by-run basis.

3 Cosmic "Muon" Selection

To select the cosmic "muon" (i.e., particle that are close to MIP) tracks in the certain segment in some of the columns, we require the high amplitudes (viz., $adc > 70$) in the 2 remaining segments of the column of interest as well as low amplitudes (viz., $adc < 10$) in all segments of the left neighbour and the right neighbour columns (see Fig.4). Such a criterion suppresses the events with a shower and picks out vertical-oriented particle tracks in the calorimeter; it selects about 15-20% of the total number of events in the run (see Fig.5).

4 Amplitude Spectra

Typical amplitude spectra (after pedestal subtraction) from the North and South PMTs are shown in Fig.8. For photoelectron analysis of these single-end amplitude spectra, we followed the general ideas described in the paper [1]. In the high-intensity-light-source limit, the authors

describe the PMT amplitude spectrum from LED standard light pulses as a convolution of the Poisson distribution (that represents the photoelectron statistical fluctuation) and the Gaussian functions (that represents PMT gain resolution and the pedestal contribution).

In our case of electromagnetic calorimeter, the widths of the observed spectra are the result of both the fluctuations in the number of photoelectons (North-South uncorrelated effect) and the variations in the enegry deposited in the calorimeter segment (North-South correlated effect). To address this extra-broadening of the spectra, we simulated the energy deposition from the muons in the realistic model of the calorimeter using FLUKA 2006.3b program [2,3]. In the simulation, the primary muons polar angles were seeded according to the $cos^2(\theta)$ law, the azimuth angles as well as the coordinates of the emitting points (in the top trigger paddle limits) were seeded uniformly, and (to meet the trigger conditions) the hits of the bottom trigger paddle were required (see Fig.6). The simulated Birks-corrected energy depositions in the fibers summed over each of the calorimeter segment were recorded on event-by-event basis, and the "muon" selection cuts were applied. The typical resulting spectra $F(\Delta E)$ of energy deposited in the calorimeter segments by 5 GeV/c muons are shown in Fig.7; mean energy depositions $\overline{\Delta E}$ were calculated for each of the segments.

Using the simulated $F(\Delta E)$ functions, we fit experimental pedestal-subtracted ADC spectra to the function (red line in Fig.8):

$$f(x) \sim \int_{E_{min}}^{E_{max}} d(\Delta E) \left[F(\Delta E) \cdot \sum_{n=0}^{n_{max}} Poi(n,\, k \cdot \Delta E) \cdot Gau(x, n, \sigma_n) \right], \qquad (1)$$

where $Poi(n,\, k \cdot \Delta E)$ is the Poisson distribution with the expected value of $(k \cdot \Delta E)$, $k = (N_{pe}/\overline{\Delta E})$ is energy-to-NPE conversion factor, $Gau(x, n, \sigma_n)$ is the Normal distribution with the mean value of n and standard deviation of σ_n. We estimated the value of PMT gain resolution σ_n for n photoelectrons using the formula (see [1,4]):

$$\sigma_n^2 \;=\; n\frac{g^m - 1}{g^m(g-1)} \;\approx\; n\frac{1}{g-1}, \qquad (2)$$

where g is the mean dynode secondary emission coefficient (in our case, it's about 4.2), and m is the number of dynodes in the PMT.

Typical fits to the single-end ADC spectra are shown in Fig.8 as red lines. Fig.9 shows the distribution of χ^2/NDF values from 144 (= 18 segments×2 ends×4 runs) fits. A summary of the average numbers of photoelectrons extracted sector-by-sector from single-end ADC spectra in four cosmics runs is shown in Figs.10-13. The mean number of photoelectrons (viz., $N_{pe}^{mean} \equiv \sqrt{N_{pe}^{North} \cdot N_{pe}^{South}}$), averaged over all segments and all runs, is 25.5±0.7 . A strong correlation between mean amplitudes (averaged on run-by-run basis) and correspondent extracted mean numbers of photoelectrons is shown in Fig.14; the close-to-linear dependence proves undoubtedly that **the cosmic ray data analysis does reliably extract the number of photoelectrons**.

5 Ratio Spectra

Another way to remove most of the dependence on the energy deposition variations and extract the mean number of photoelectrons from cosmic "muons" is to use the spectra of North/South amplitudes ratio (see Fig.15). We suppose that each of the amplitude spectra has the Poisson-type shape; consequently, the ratio spectra were fitted to the function (red line in Fig.15):

$$f(r) \sim \int P(x,\, N_{pe} \cdot \sqrt{R}) \cdot [\frac{1}{r}\, P(\frac{x}{r},\, N_{pe} \,/\, \sqrt{R})]\, [\frac{x}{r}\, dx], \qquad (3)$$

where r is a North/South amplitudes ratio, R is an average North/South amplitudes ratio, N_{pe} is the average number of photoelectrons, P is a Poisson-type probability:

$$P(x, N) = e^{-N} \cdot N^x / \Gamma(x+1), \tag{4}$$

and the $(1/r)$ and (x/r) factors are needed to perform the integration over the uniform r-bins.

A summary of the average numbers of photoelectrons extracted sector-by-sector from the ratio spectra in four cosmics runs is shown in Fig.16. The N_{pe} values of 21.43±1.02, 23.93±0.93, 20.92±0.70, and 20.83±0.75 are extracted from the runs 2458, 2459, 2475, and 2476, correspondingly; these values are in a good agreement. The number of photoelectrons, averaged over all segments and all runs, is 22.0±0.9 .

Comparison of the results from the single-end spectra analysis (left panel) and the ratio spectra analysis (right panel) from four cosmics runs is shown in Fig.17.(For the single-end spectra analysis, we used the geometrical mean of the numbers of photoelectrons from both ends ($\equiv \sqrt{N_{pe}^{North} \cdot N_{pe}^{South}}$).) Both results are in a reasonably good agreement (see Fig.18), though a slight underestimation of the mean number of photoelectrons from the ratio spectra analysis originates (most probably) from a non-complete compensation of the energy-deposition distribution.

6 Correction of Extracted N_{pe} on Non-Constant Light Transmission and Fiber-PMT Coupling

Recently, concerns were raised in a report [5] that the number of photoelectrons extracted from the width of amplitude spectra is enormously distorted with fiber-to-fiber non-uniformity in fiber-PMT coupling. In this section, we address these concerns with a realistic estimation of the required correction that should be applied to the extracted number of photoelectrons.

Let us assume that the cosmic muon deposits energy ϵ_i in the i-th fiber, this energy is converted into the light with a constant factor y, and the light is transported to the PMT photocathode with a transmission/coupling factor C_i. The number of photons that arrive at the PMT photocathode from n fibers:

$$p_n = y \sum_i^n (C_i \epsilon_i) \tag{5}$$

fluctuates with a variation:

$$V(p_n) = y^2 \sum_i^n [C_i^2 \, V(\epsilon_i) \, + \, \epsilon_i^2 \, V(C_i)], \tag{6}$$

where $V(\epsilon_i)$ and $V(C_i)$ are variations for the values ϵ_i and C_i, respectively. Each of the C_i factors can be represented via a mean transmission/coupling factor $\overline{C}$ and a fiber-to-fiber deviation δ_{Ci} from the mean value (i.e., $\sum \delta_{Ci} = 0$), so:

$$\sum_i^n C_i^2 \, = \, \sum_i^n (\overline{C} \, + \, \delta_{Ci})^2 \, = \, \sum_i^n \overline{C}^2 \, + \, 2 \, \overline{C} \sum_i^n \delta_{Ci} \, + \, \sum_i^n \delta_{Ci}^2 \, = \, n \, \overline{C}^2 \, + \, n \, V(C_i) \tag{7}$$

Similar representation of the ϵ_i energy deposition via a mean energy deposition (E/n) in the fiber and a fiber-to-fiber deviation $\delta_{\epsilon i}$ leads to:

$$\sum_i^n \epsilon_i^2 \, = \, \sum_i^n \left(\frac{E}{n} \, + \, \delta_{\epsilon i} \right)^2 \, = \, \sum_i^n \left(\frac{E}{n} \right)^2 \, + \, 2 \left(\frac{E}{n} \right) \sum_i^n \delta_{\epsilon i} \, + \, \sum_i^n \delta_{\epsilon i}^2 \, = \, \left(\frac{E^2}{n} \right) \, + \, n \, V(\epsilon_i) \tag{8}$$

Taking into account that the variation of the total energy deposited in n fibers is:

$$V(E) \,=\, n\, V(\epsilon_i) \tag{9}$$

and

$$V(C) \,=\, V(C_i), \tag{10}$$

we can reduce the variation $V(p_n)$ to the following form:

$$V(p_n) \,=\, y^2 \left[V(E)\, \overline{C}^2 \,+\, V(E)\, V(C) \,+\, V(C)\, \frac{E^2}{n} \,+\, V(E)\, V(C) \right] \,=$$

$$=\, y^2\, \overline{C}^2 \, \left[V(E) \,+\, \frac{V(C)}{\overline{C}^2} \left(2\, V(E) \,+\, \frac{E^2}{n} \right) \right] \tag{11}$$

Please notice a disagreement between formula (11) above and the corresponding formula (4) in the report [5]: here, formula (11) does not contain a factor of 2 in the (E^2/n) term.

From formula (11), we can conclude that the fiber-to-fiber non-uniformity in light transmission and fiber-PMT coupling can be taken into account as an additional effective broadening to the energy-deposition spectrum that should be estimated with the realistic cosmic-ray parameters. Within the 3.8×3.8 cm^2 readout window, a PMT collects the light from n=30 layers of fibers. The simulation for high-energy muons (see "Amplitude Spectra" Section and right panel of Fig.7) gives distribution of total energy deposited in the 30 layers of fibers with a mean value E of about 5.0 MeV and RMS value [$\equiv \sqrt{V(E)}$] of about 1.2 MeV; these values do not change significantly with the variation of the cosmic muon energy. The effective broadening of the energy deposition distribution [$\equiv \sqrt{V(p_n)/V_0(p_n)}$, where $V_0(p_n) = y^2 \overline{C} V(E)$] calculated as a function of the assumed relative tramsmission/coupling dispersion [$\equiv \sqrt{V(C)}/\overline{C}$] is shown in the top panel of Fig.19; the bottom panel of the Fig.19 shows the mean number of photoelectrons extracted from the single-end spectra analysis as a function of the assumed relative transmission/coupling dispersion. The analysis demonstrates that the realistic fiber transmission/coupling dispersion up to 10-15% leads to a **negligible correction** in the extracted number of photoelectrons; even a pessimistic assumption of 50% dispersion requires a correstion for 7 additional photoelectrons only. Qualitatively, we read out the sum of the signals from 30 fibers (viz., we make an effective signal average over 30 fibers), so even large dispersions in individual fiber transmission/coupling are reduced by significant factor in the average value.

7 Attenuation Length of the Light in BCal

Significantly unbalanced PMTs (see Fig.20) require sector-by-sector extraction of the light attenuation length in the BCal. Fig.21 shows fit of typical Mean-Amplitude-vs-Trigger-Position dependences for one of the North and one of the South PMTs (left and right panels, correspondently) to the exponent function. Also, Amplitude-Ratio-vs-Trigger-Position dependences were used for the sector-by-sector extraction of the light attenuation length in the BCal (see Fig.22).

Summaries of the attenuation lengths of the light in the BCal extracted from amplitudes from North or South PMTs and from the ratio of North/South amplitudes are shown in Fig.23 (left and right panels, correspondently). Mean light attenuation lengths extracted using "one-side" technique (229.1±2.5 cm) and using the "ratio" technique (235.4±1.7 cm) are in a good agreement.

References

[1] I. Chirikov-Zorin et al. Nucl. Instrum. Meth. **A456**, 310 (2001).

[2] A. Fasso, A. Ferrari, P.R. Sala, Electron-Photon Transport in FLUKA: Status, Proceedings of the Monte Carlo 2000 Conference, Lisbon, October 23-26, 2000, A. Kling, F. Barao, M. Nakagawa, L. Tavora, P. Vaz eds., Springer-Verlag Berlin, pp. 159-164 (2001).

[3] A. Fasso, A. Ferrari, J. Ranft, P.R. Sala, FLUKA: Status and Perspective for Hadronic Applications, Proceedings of the Monte Carlo 2000 Conference, Lisbon, October 23-26, 2000, A. Kling, F. Barao, M. Nakagawa, L. Tavora, P. Vaz eds., Springer-Verlag Berlin, pp. 955-960 (2001).

[4] R. Bollmann et al. Nucl. Instrum. Meth. **A342**, 466 (1994).

[5] R.T. Jones, "On the Measurement of BCAL Photoelectron Statistics", GlueX-doc-867 (2007).

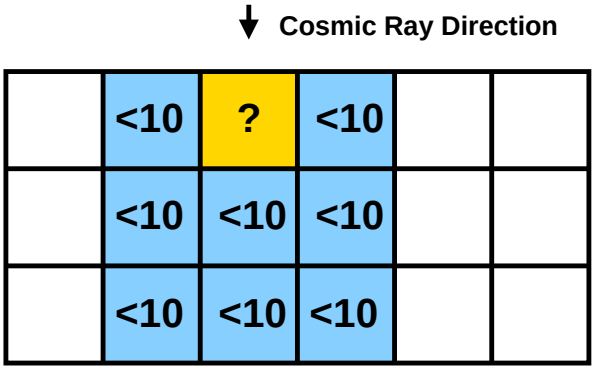

Figure 1: Selection of pedestal events in BCal cosmics data.

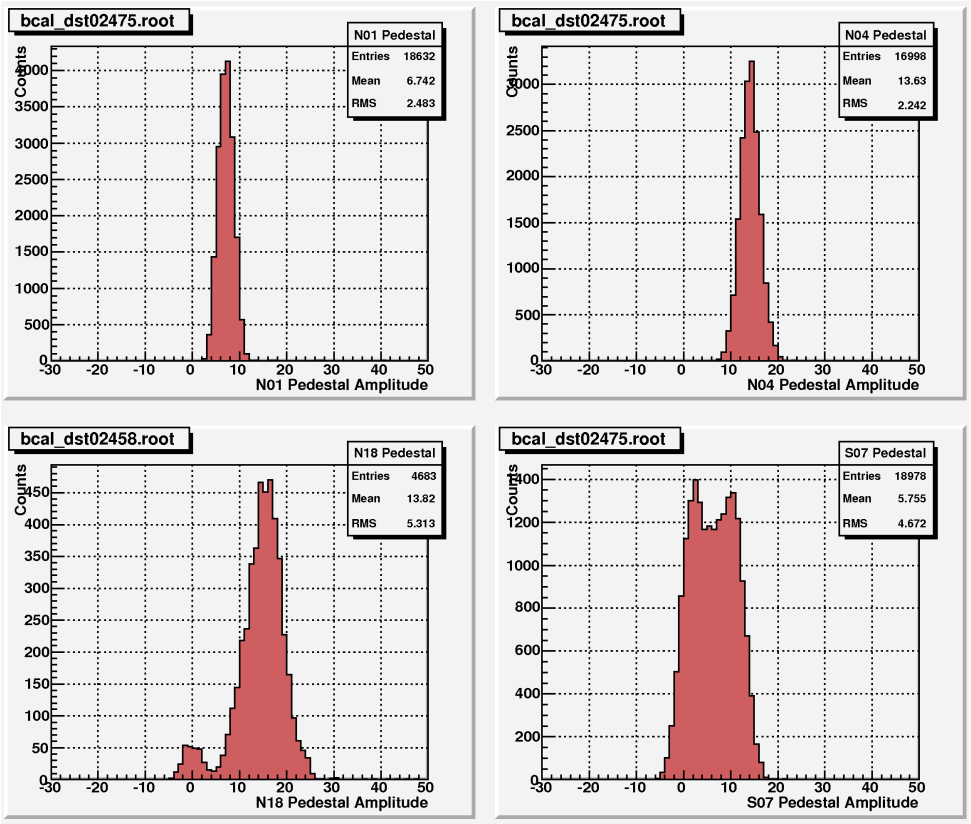

Figure 2: Typical (top-left panel) and abnormal (other panels) pedestal spectra.

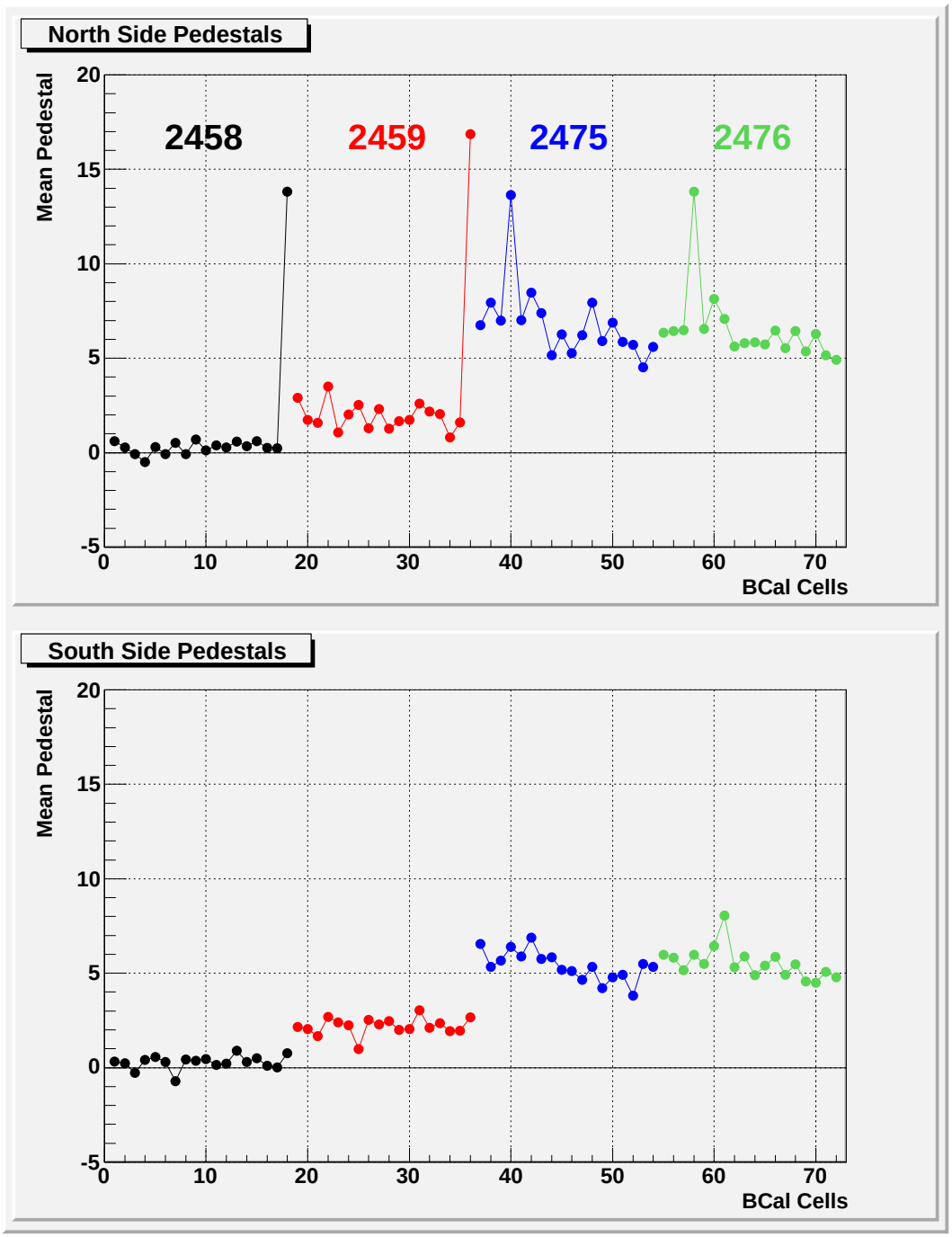

Figure 3: Mean pedestal values extracted from all 18 segments in 4 runs for North-side PMTs (top panel) and South-side PMTs (bottom panel).

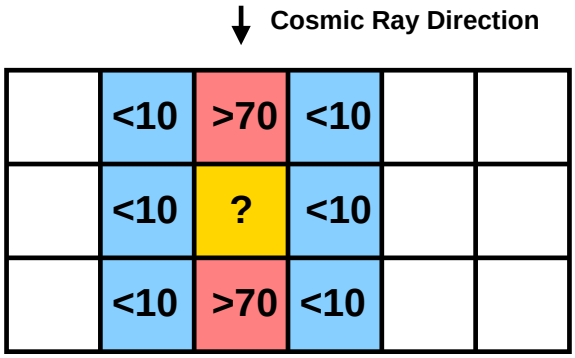

Figure 4: Selection of "muon" events in BCal cosmics data.

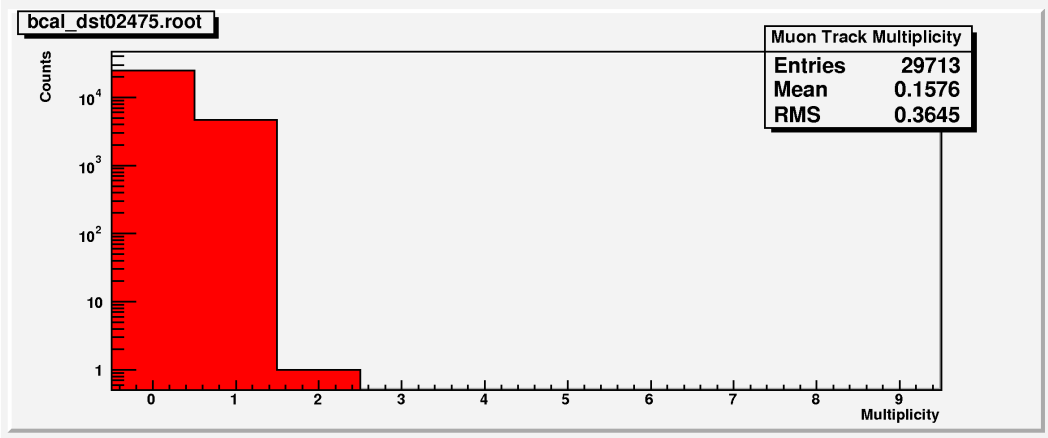

Figure 5: "Muon" event multiplicity in the run 2475.

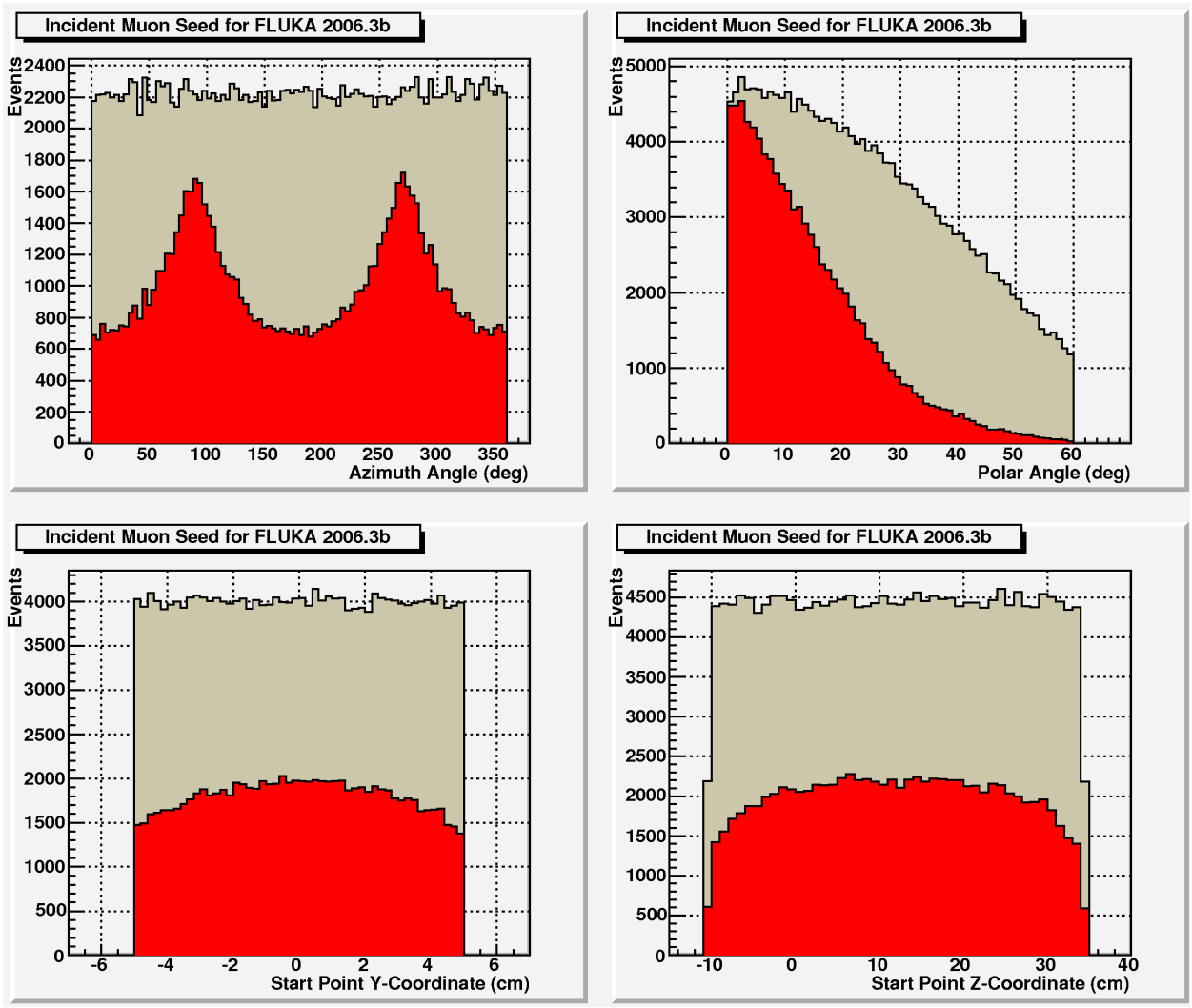

Figure 6: The incident muon parameters seed for the simulation with FLUKA 2006.3b program. Top-left panel: azimuth angle. Top-right panel: polar angle (viz., the angle between the muons momentum and a vertical direction). Bottom panels: Y and Z position of the muon start point inside top trigger paddle. Gray (red) histograms correspond to the events before (after) the hit in the bottom trigger paddle was required. The events from red histograms were used as the input for FLUKA simulation.

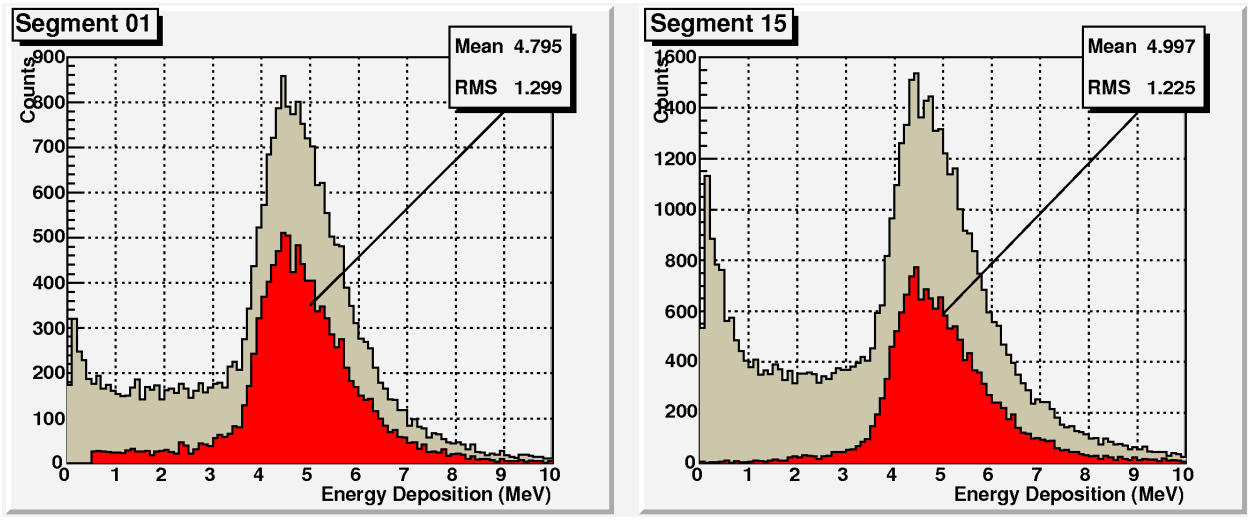

Figure 7: Typical spectra of energy deposited in the calorimeter segments by 5 GeV/c muons before (gray histograms) and after (red histograms) "muon" selection cuts were applied. (Result of the simulation with FLUKA 2006.3b program.) Left panel represents the segment #1 located at the edge of the calorimeter, and the right panel corresponds to the segment #15 in the middle of the calorimeter. Statistics boxes correspond to the red histograms.

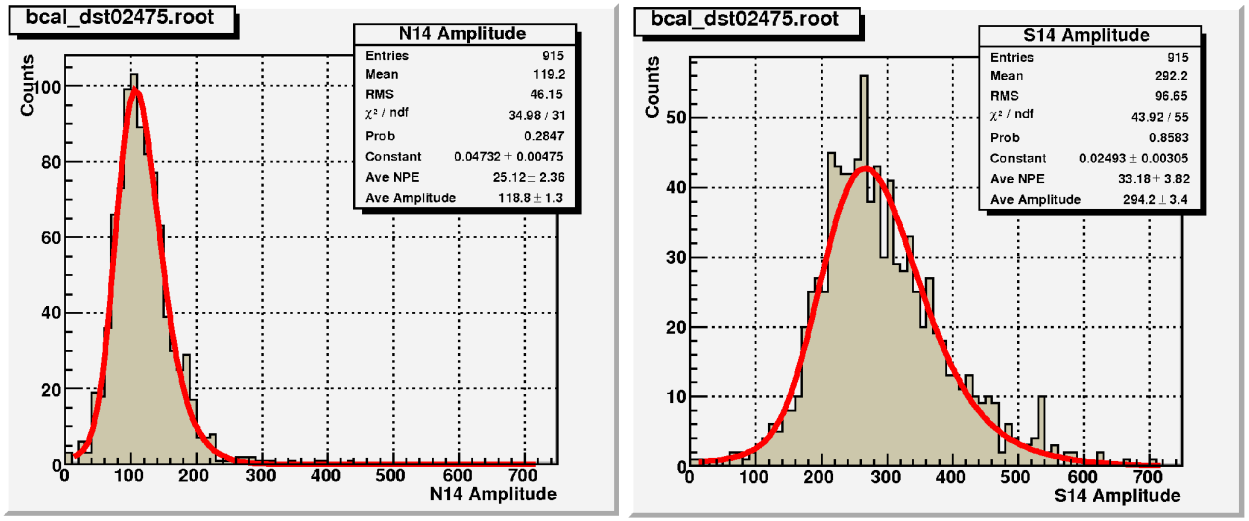

Figure 8: Typical amplitude spectra from the North (left panel) and South (right panel) PMTs in the run 2475. The red lines are the fits to the spectra (see Eq. 1).

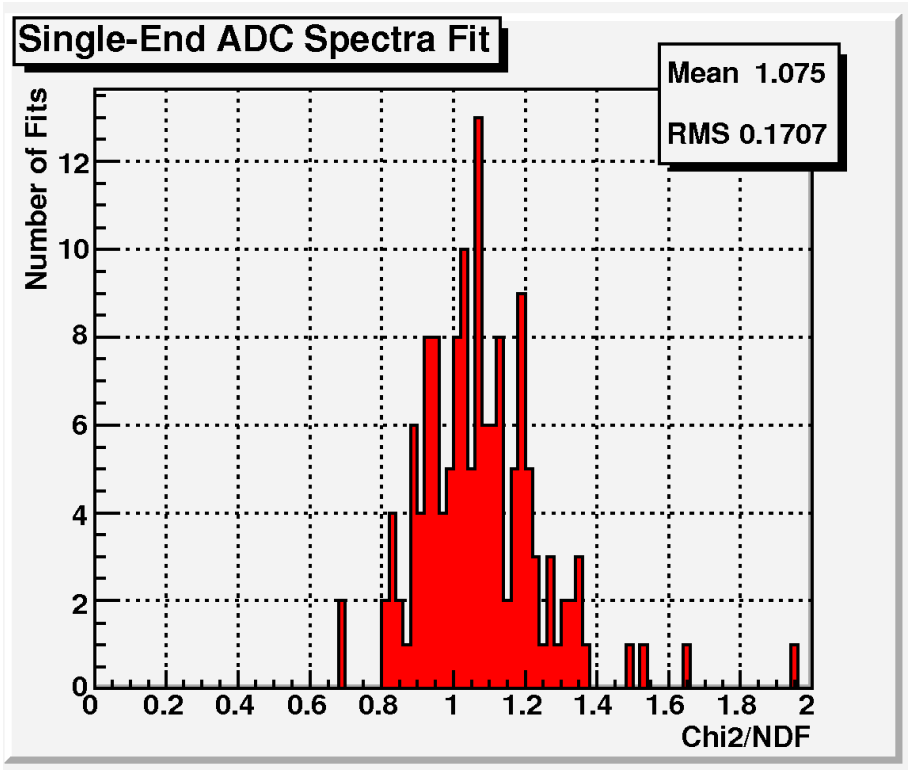

Figure 9: Distribution of χ^2/NDF values from 144 (= 18 segments×2 ends×4 runs) fits.

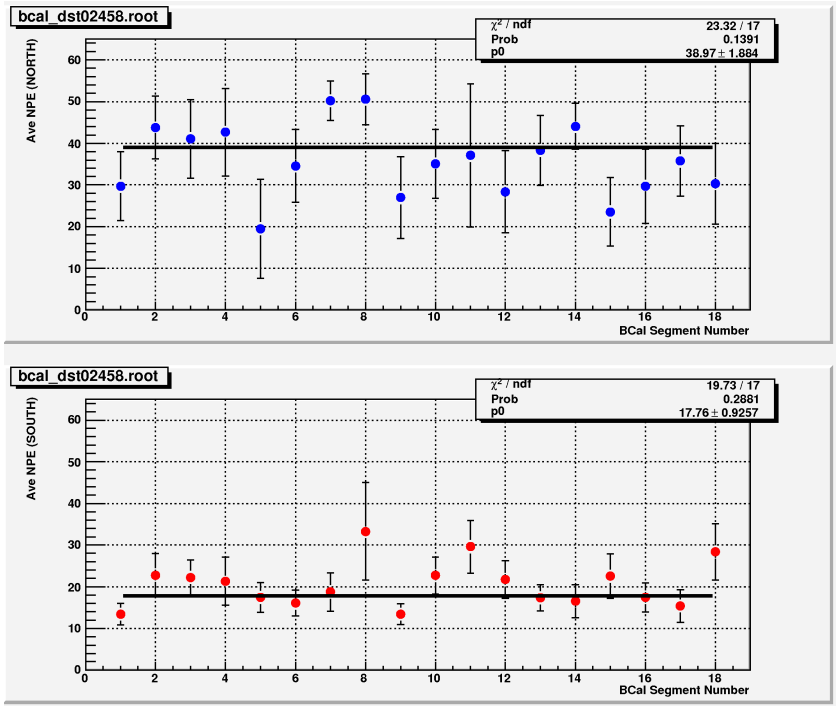

Figure 10: Average number of photoelectrons (sector-by-sector) extracted from the fit parameters of the single-end amplitude spectra in the run #2458. Top panel corresponds to the North-side readout, and the bottom panel corresponds to the South-side readout.

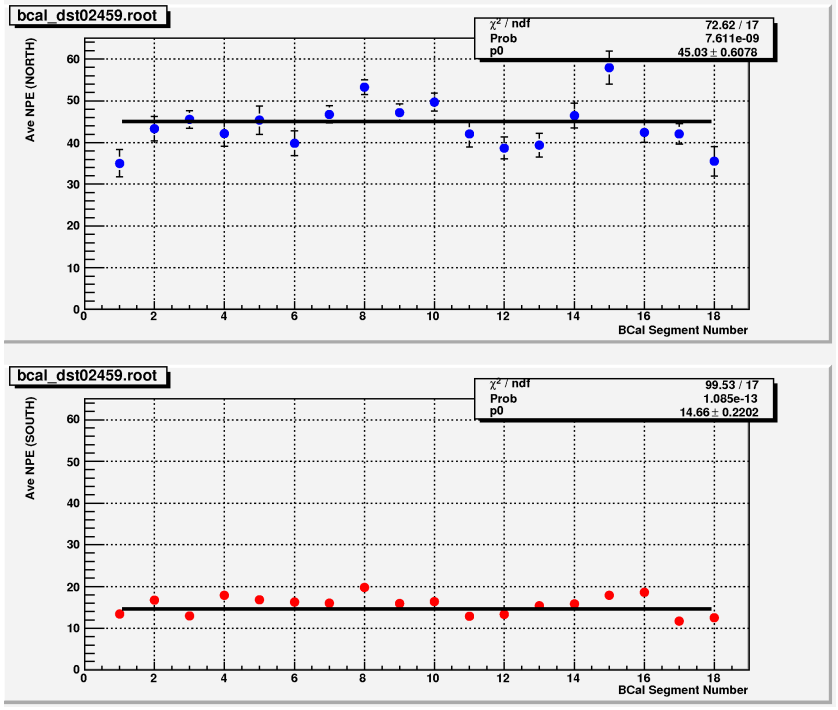

Figure 11: Average number of photoelectrons (sector-by-sector) extracted from the fit parameters of the single-end amplitude spectra in the run #2459. Top panel corresponds to the North-side readout, and the bottom panel corresponds to the South-side readout.

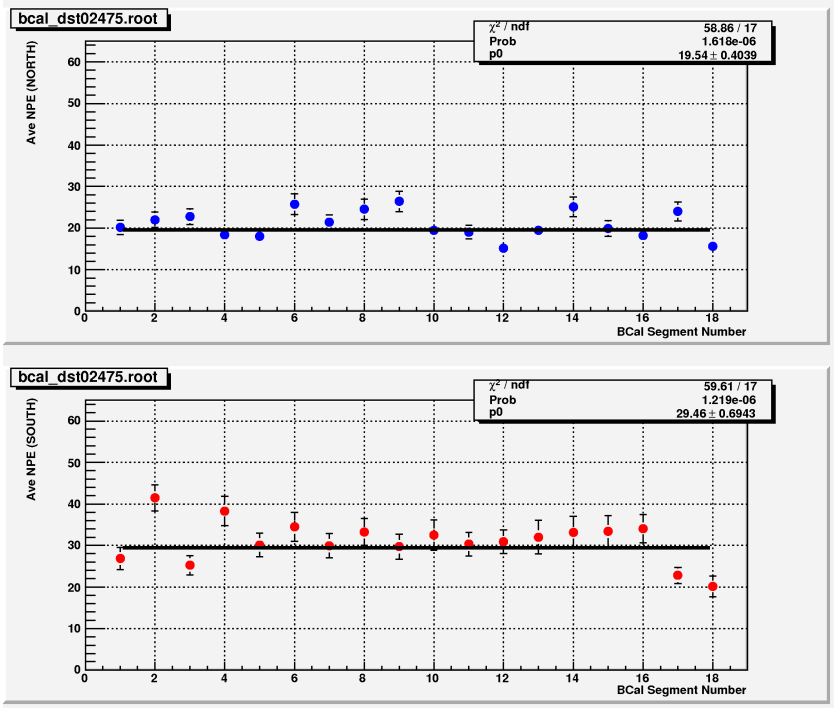

Figure 12: Average number of photoelectrons (sector-by-sector) extracted from the fit parameters of the single-end amplitude spectra in the run #2475. Top panel corresponds to the North-side readout, and the bottom panel corresponds to the South-side readout.

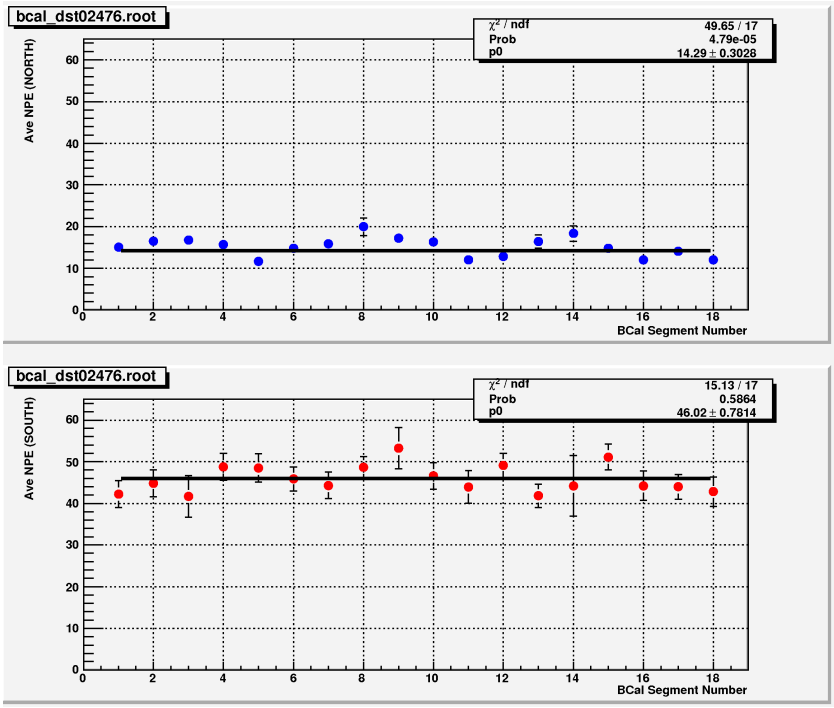

Figure 13: Average number of photoelectrons (sector-by-sector) extracted from the fit parameters of the single-end amplitude spectra in the run #2476. Top panel corresponds to the North-side readout, and the bottom panel corresponds to the South-side readout.

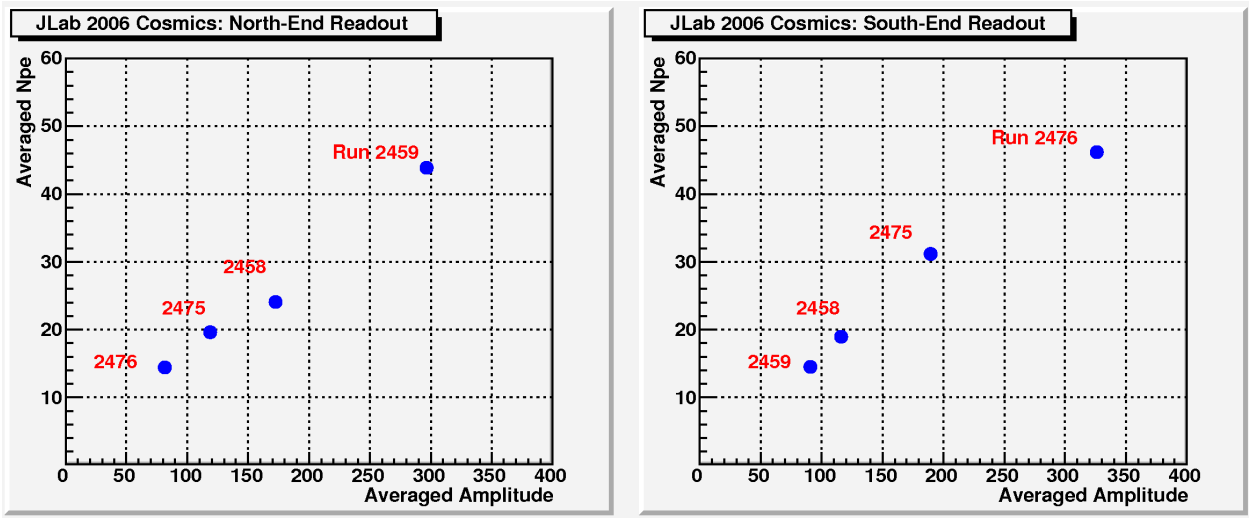

Figure 14: Correlation between mean amplitudes (averaged over segments on run-by-run basis) and correspondent extracted mean numbers of photoelectrons.

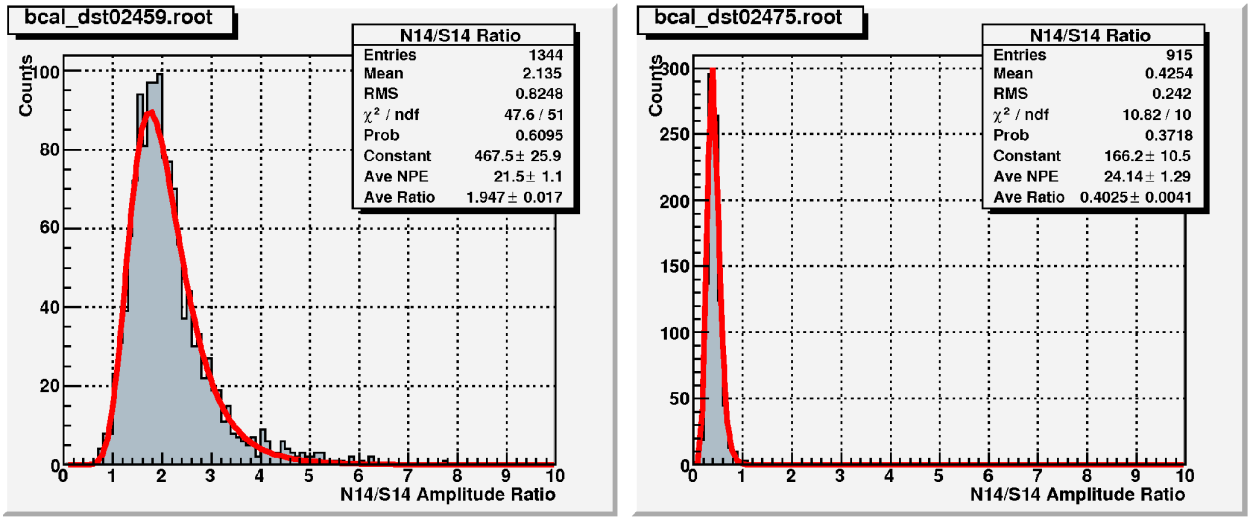

Figure 15: Typical ratio spectra in the run 2459 (left panel) and in the run 2475 (right panel). The red lines are the fits to the spectra (see Eq. 3).

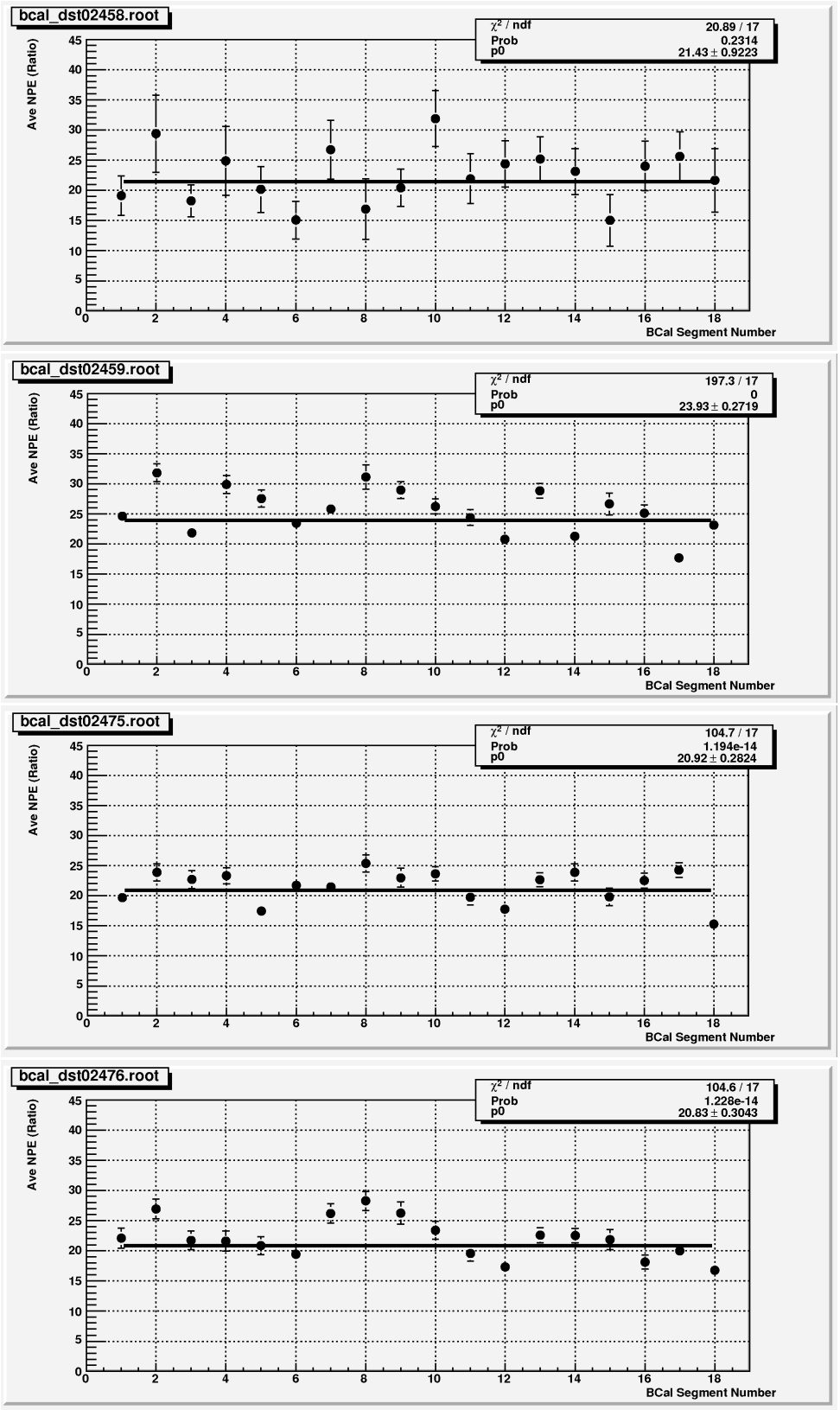

Figure 16: Average number of photoelectrons (sector-by-sector) extracted from the fit parameters of the ratio spectra for four cosmics runs.

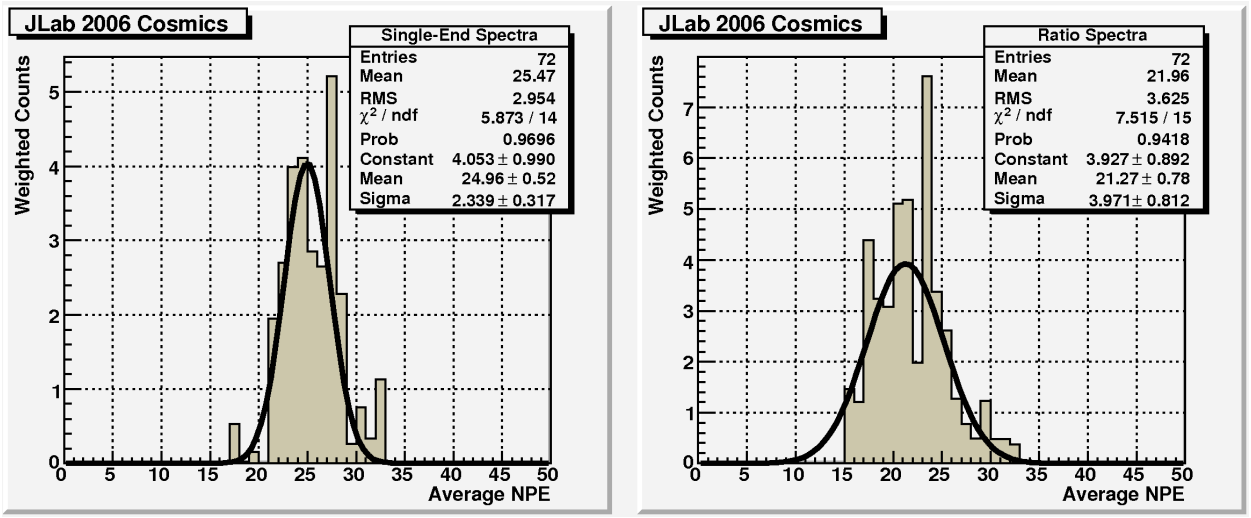

Figure 17: Comparison of the results from the single-end spectra analysis (left panel) and the ratio spectra analysis (right panel) from four cosmics runs. For the single-end spectra analysis, the mean number of photoelectrons ($\equiv \sqrt{N_{pe}^{North} \cdot N_{pe}^{South}}$) is shown.

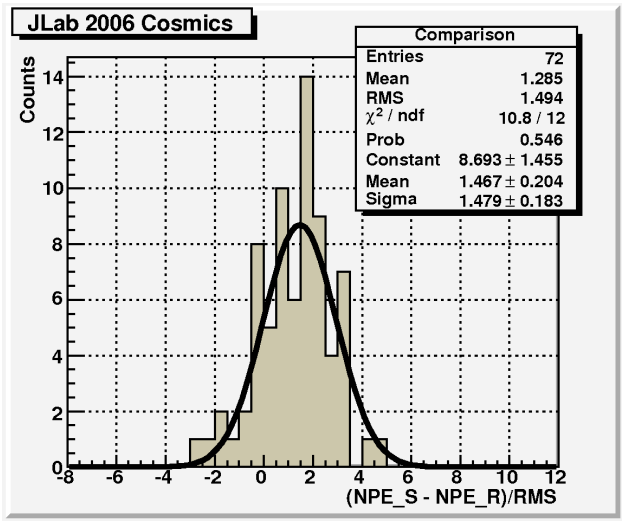

Figure 18: Difference between the results from the single-end spectra analysis and the ratio spectra analysis in the units of the measurement errors (from four cosmics runs).

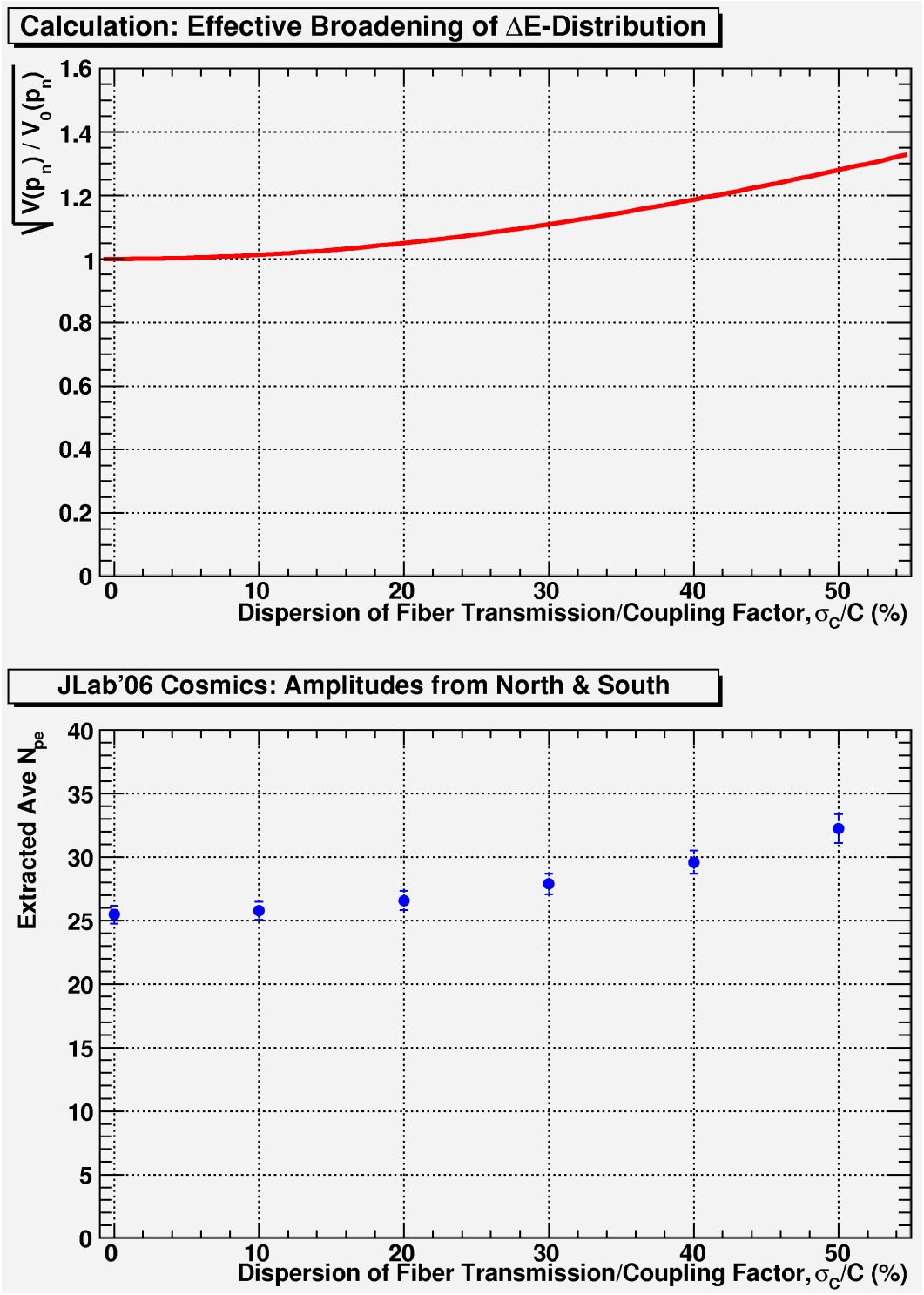

Figure 19: Calculated effective broadening of Δ-E distribution (top panel) and the number of photoelectrons extracted from JLab'06 cosmic data (bottom panel) as a function of assumed dispersion of fiber transition/coupling factor.

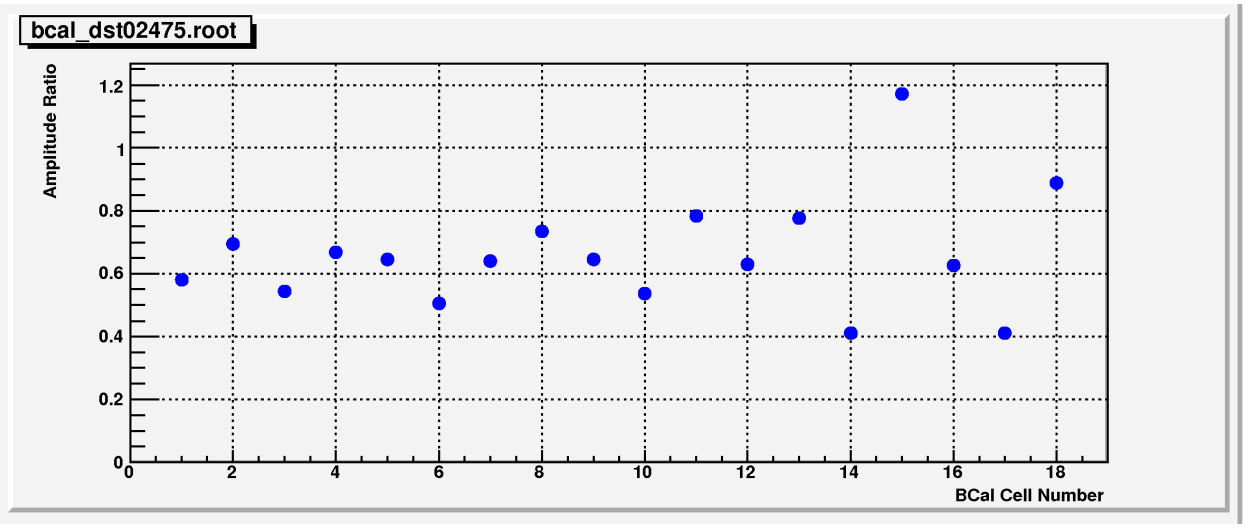

Figure 20: Sector-by-sector mean values of North/South amplitudes ratios in the run 2475. Note the significant spread.

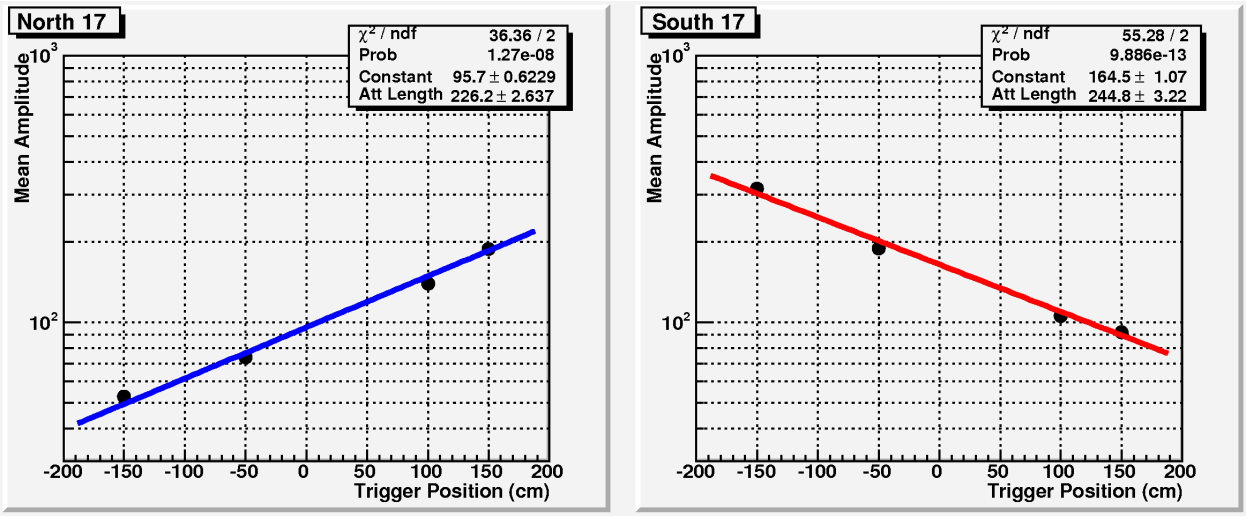

Figure 21: Extraction of the attenuation length of the light in the BCal using amplitudes from North or South PMTs.

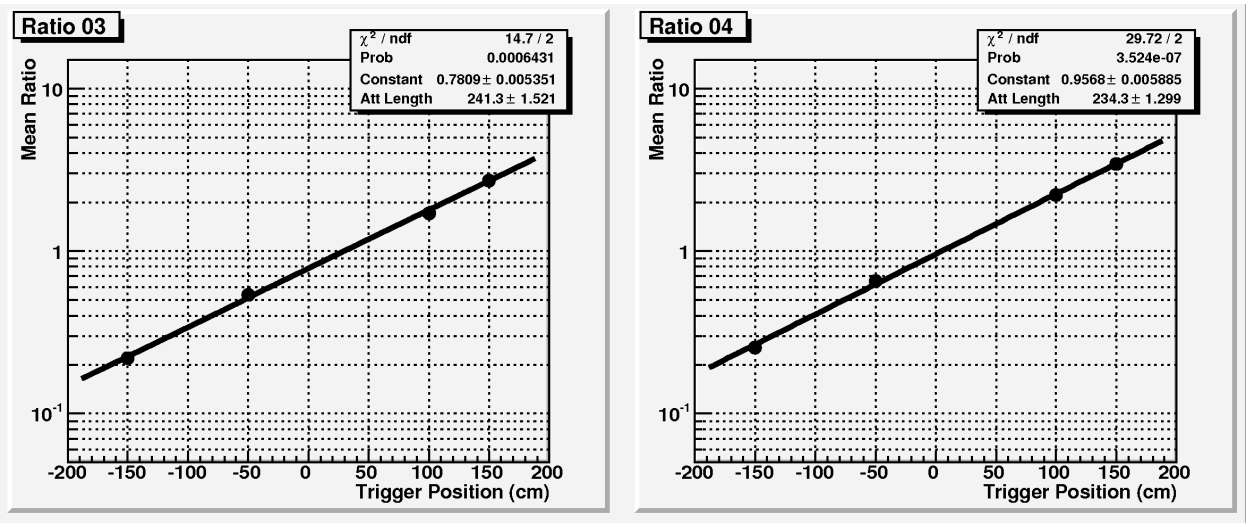

Figure 22: Extraction of the attenuation length of the light in the BCal using the ratio of amplitudes from North and South PMTs.

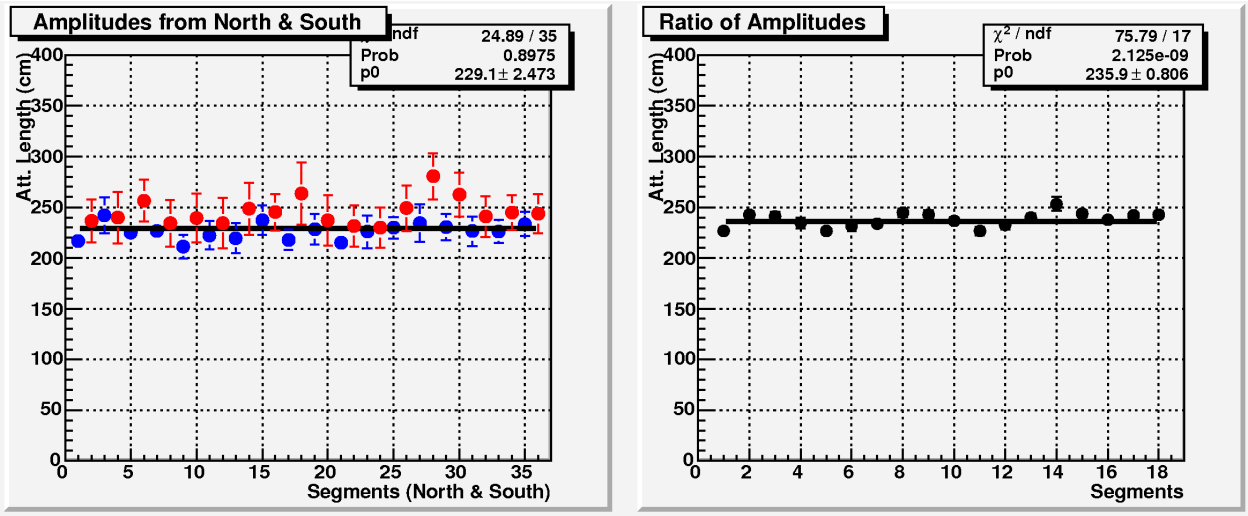

Figure 23: Summary of the attenuation lengths of the light in the BCal extracted from amplitudes from North or South PMTs (left pannel: blue symbols are for the attenuation length values extracted from the North PMT amplitudes, red symbols are for the values extracted from the South PMT amplitudes; fit made to whole data set) and from the ratio of North/South amplitudes (right panel).